

CHAPTER 160

DESIGN, ANALYSIS AND FIELD TEST OF A DYNAMIC FLOATING BREAKWATER

D. J. Agerton¹, G. H. Savage², K. C. Stotz³

Interest in floating breakwaters has been generated in recent years because the concept offers the potential of providing a less expensive alternative to traditional, solid wall type barriers for providing permanent wave protection to the thousands of new recreational boat harbors and marinas that have been built in the past 20 years. Also, they may be able to provide temporary, mobile wave protection during construction and installation of offshore facilities for oil transfer and production operations, defense facilities and other offshore structures in deeper water (depths exceeding 50 to 100 feet).

The engineering director of one of the largest and most active offshore oil producing companies recently stated that they would be willing to pay up to \$6 million for a mobile, floating breakwater that had the proven capability to significantly reduce risks due to wave action during offshore erection in the North Sea or elsewhere. Considering the investment in just one deep water oil production platform already exceeds \$100,000,000, the worth of such a reusable, wave protection system during the critical erection period of a platform should be large.

The tethered float concept - a dynamic breakwater: In 1974, Seymour and Isaacs (1) introduced the concept of a submerged, tethered float breakwater, an approach that shows promise of being able to attenuate long period, large, deep-water, storm waves at a sufficiently low cost to be feasible. The system is made up of an array of independently moored, spherical buoys submerged just below the water surface (See Fig. 1). Seymour and Isaacs (1) proposed that, with proper specification of tether length and buoy size, each buoy would have a resonant frequency near that of the anticipated predominant waves for a given location. Owing to their dynamic response, it seemed possible to cause the buoys to pendulate back and forth in the incoming waves out of phase with the wave orbital motions; thus the name: Dynamic Breakwater. The effect of this wave excited buoy motion would be to transform wave energy into water turbulence and then heat in the wake of the buoy.

¹Engineering Ph.D. Candidate, University of New Hampshire.

²Professor of Engineering, University of New Hampshire.

³Associate Professor of Electrical Engineering, University of New Hampshire.

Additions and modifications to the tethered float concept: Before and during Isaacs's and Seymour's work Savage and others (2,3,4) had been investigating solid rubber filaments for various buoy mooring applications, and suggested that the use of such moorings would improve the survivability and longevity of such a floating breakwater. Follow-up of this idea soon presented the possibility of significantly increasing the wave attenuation efficiency of the Isaacs-Seymour system. A buoy tether's spring constant might be chosen so it resonated with the predominate wave frequency in the vertical as well as in the horizontal direction. Thus, each buoy could be expected to create more turbulence and dissipate more energy than an inelastically-tethered one. Wave tank model studies of this approach with a single elastically-tethered buoy in 1974 confirmed the possibility of achieving orbital buoy response out of phase with the orbital water particle motion, and encouraged us to proceed.

Research objectives and scope: The three aspects of our investigation were:

- 1) to compare the dynamic response and wave attenuation by tethered buoys with different tether elasticities, float shapes, spacings, and levels of submergence in a wave tank,
- 2) to develop predictive mathematical models of buoy response and wave attenuation in wave tank and field tests,
- 3) to conduct a large enough lake scale model test so that the Reynolds number and period parameter would be large enough for fully turbulent wake conditions to be developed in the buoy field; a condition that we expected to prevail in a full scale system.

The last objective seemed the most significant because successful achievement of fully turbulent flow conditions in a model would permit model results to be used to predict full scale breakwater performance. At the time no other field tests had been carried out for a tethered float array.

WAVE TANK TESTS

The wave tank tests were conducted in the ship model towing facility of the Massachusetts Institute of Technology, Cambridge, Massachusetts. One set of tests measured the dynamic response of a single buoy to sinusoidal wave of various heights and frequencies. Several different shapes of buoys and tethers with different spring constants were used. Buoy response was recorded by means of an optical displacement follower which could continually track the oscillating buoy using only light and no instruments in direct contact with the buoy or its tether. The three float shapes tested were a sphere, a sphere with a concentric disk around its girth (a "Saturn ring"), and an egg. The scale size of the buoy was assumed from Seymour and Isaacs (1) work with a sphere which had shown that "reasonable diameters for the breakwater will be of the same order as the significant wave height".

The buoy shape and tether selected were a sphere with a tether with a low spring constant so that the buoy response to the significant waves in our model sea state and water depth was a near circular orbit (See Fig. 2). The preliminary mathematical model of the system had indicated that such an orbital response would result in the greatest energy dissipation due to form drag for a single buoy. The spherical buoy shape was selected over the other two tested because it was the shape that gave significant vertical as well as horizontal response; *i.e.* near-circular buoy motion.

We then constructed arrays of both wire and elastically-tether buoys across the wave tank and subjected these model dynamic breakwaters to both regular and irregular seas (See Fig. 3). The incident and attenuated waves were measured and recorded and the respective wave energies were calculated. These wave tank breakwater model tests gave results that supported the validity of our first analytical prediction models that elastically-tethered floats dissipated more energy than wire-tethered ones. Other results are shown in Fig. 4.

MATHEMATICAL MODELING

Modeling an elastically-tethered dynamic breakwater requires four steps: (a) writing equations of motion for a tethered buoy in two dimensions; (b) solving those equations for buoy relative velocity; (c) computing the rate of energy dissipation (drag power) of a row of buoys; (d) compounding the drag power row-by-row through the array. In light of the two-dimensional nature of the problem and the complexities introduced by elastic tethers, we did not rely solely on the simplified linear-model approach of Seymour (5). Solution to the non-linear, coupled problem is detailed in a dissertation by Agerton (6) and summarized below. It is a solution of the general case; not restricted to a wire-tethered system.

Modeling wave forces: Force on a fixed object in one-dimensional oscillatory flow can be formulated by the Morison equation as the sum of nonlinear drag and inertial components (7). Frontal area A and flow coefficients C_D and C_M are considered constant.

$$F = F_D + F_I \quad (1)$$

$$F = \frac{1}{2} \rho A C_D |u|u + \rho V_o (1 + C_M) \dot{u} \quad (2)$$

In one-dimensional oscillatory flow, the only dimensionless parameter correlated with drag and mass coefficient is period parameter (8,9) defined as:

$$PP = U_m \tau / d = 2\pi a / d \quad (3)$$

where a is the amplitude of water motion relative to the object. However, the relationship between flow parameters, object dimensions, and flow-force coefficients is not well understood, particularly in two-

dimensional oscillatory flow as would occur in waves in a field experiment. Furthermore, if the amplitude to diameter ratio were the only important parameter, then the scaling of drag forces would present no problem. We have heard no investigator propose that to be the case.

Complexity of the problem increases for two-dimensional flow problems -- as occur for waves acting on a submerged tethered sphere or horizontal cylinder parallel to the wave crests. In such cases, the turbulent wake would appear to rotate around the object during the wave cycle. The vector force can be written by the Morison formulation. Area presented to the flow is the same from all directions. Also, it is assumed C_D and C_M do not change with direction.

$$\vec{F} = \vec{F}_D + \vec{F}_I \tag{4}$$

$$\vec{F} = \frac{1}{2} \rho A C_D |\vec{r}| \vec{r} + M_W (1 + C_M) \ddot{\vec{r}} \tag{5}$$

where \vec{r} is the relative velocity of the fluid and $\ddot{\vec{r}}$ is its relative acceleration. Both can be resolved into horizontal and vertical components. The one and two-dimensional formulations are compared below:

Two-dimensional formulation

One-dimensional formulation

$$F_x = D u \sqrt{u^2 + v^2} + N \dot{u} \tag{6}$$

$$F_x = D |u| u + N \dot{u} \tag{6}$$

$$F_y = D v \sqrt{u^2 + v^2} + N \dot{v} \tag{7}$$

$$F_y = D |v| v + N \dot{v} \tag{7}$$

If only maximum force predictions are of interest, both formulations give the same result. However, when considering wave-force history and energy dissipation, the two-dimensional problem should be formulated as such or justifiably de-coupled into a pair of one-dimensional equations.

By computing the drag work during a wave cycle, one finds that about 15% less energy is dissipated by the one-dimensional formulation. A similar comparison for an elastically tethered sphere is not as simply accomplished because the object has both horizontal and vertical relative velocity whose magnitudes are not necessarily equal. However, the 15% difference in calculated dissipation represents the maximum.

Coefficients of mass and drag: Data on which to base estimates of drag and mass coefficients for spheres in waves are neither plentiful nor consistent. Seymour (5) was first to estimate flow coefficients for tethered spheres in irregular waves in both the laboratory and the ocean. He concluded that at values of rms a/d greater than 0.80, the average C_D was constant. This indicated to him that the flow was fully turbulent -- that is, the wake was fully developed. He further observed that C_M decreased in a gradual linear fashion with increasing a/d ratio, so assuming a single value over a particular excitation spectrum was an acceptable approximation. When the sphere was less rigidly restrained, Seymour observed that C_D increased almost two-fold. He hypothesized that lateral vibration increased the width of the wake and, therefore, the form drag. Laird (10) made similar observations for cylinders. Sarpkaya (9) recently calculated C_D and C_M over a range of period para-

meters in one-dimensional oscillatory flow. The sphere was not rigidly restrained. At a/d ratios greater than about 3.0, C_D was constant at about 0.75, much higher than Seymour had measured. Below 3.0, it decreased in an almost linear fashion. In an ocean experiment, Seymour (5) inferred values of 0.35 and 0.25 for C_M and C_D respectively for a tethered sphere in two-dimensional flow. These were about 70% higher than those calculated in laboratory experiments, a difference he attributed to transverse vibration. Values of flow coefficients estimated by Seymour in the field were initially adopted to carry out the design of our experiments because he had made the only large-scale measurements in two-dimensional flow.

Modeling buoy response and energy dissipation: Fig. 5 depicts the geometry of an elastically-tethered sphere in waves. Based on wave tank observations and on the analysis of elastic tethers, articulation and catenary were assumed negligible (4,11). The working range of the elastic tether is approximately linear (11). Depending primarily on the thickness of the tether, drag forces on the mooring may be substantial. Formulating drag force on a differential section of tether whose free end moves with the velocity of the buoy \dot{x} , and integrating over the length yields:

$$F_{Dt} = \frac{1}{6} \rho A_t C_{Dt} |\dot{x}| \dot{x} \quad (8)$$

Buoyancy, acceleration, wave, and tether forces on the tethered buoy can be resolved into horizontal and vertical components, summed, and algebraically re-arranged to yield non-linear coupled equations of motion.

$$M_x \ddot{x} + D_x |\vec{r}| (\dot{x}-u) + D_t |\dot{x}| \dot{x} + T \sin(\theta) = N_x \dot{u} \quad (9)$$

$$M_y \ddot{y} + D_y |\vec{r}| (\dot{y}-v) + T \cos(\theta) - F_B = N_y \dot{v} \quad (10)$$

$$\text{where } u = a w e^{-kz} \cos(\omega t - kx) \quad v = -a w e^{-kz} \sin(\omega t - kx) \quad (11)$$

Drag power is written:

$$P_{D_x} = \frac{1}{2} \rho A C_D |\vec{r}| u_r^2 \quad P_{D_y} = \frac{1}{2} \rho A C_D |\vec{r}| v_r^2 \quad (12)$$

$$\text{where } u_r(t) = \dot{x}(t) - u(t) \quad v_r(t) = \dot{y}(t) - v(t) \quad (13)$$

$$\text{Total drag is then: } P_D = P_{D_x} + P_{D_y} \quad (14)$$

Integrated over a wave period τ , the drag power and wave power are compared to yield the proportion of wave energy dissipated by a single row of buoys. This is adjusted for buoy packing density β .

$$\lambda_1(\omega_1 a_1) = \beta \frac{\int_0^{\tau} P_D dt}{\int_0^{\tau} P_W dt} \quad (15)$$

It is assumed that the amplitude reduction is completed a short time after the buoy and water have interacted. Therefore the attenuated amplitude is the incident wave amplitude for the second row of buoys.

Through compounding successive simulations, attenuation by an array of buoys can be modeled. However, because dissipation by each row is small, large error is not incurred by assuming all rows are equally effective (6). Dissipation by an array of n rows can therefore be estimated as:

$$a_n^2/a_1^2 = (1-\xi)^n \quad (16)$$

Solving for the number of rows to provide a particular level of dissipation requires solving the equations of motion.

Solution by simulation: The IBM Continuous System Modeling Program (CSMP) was used to simulate the response of an elastically-tethered buoy. Simulation in regular waves permitted calculation of frequency response, energy dissipation, and spatial plotting of the orbiting buoy. Results indicated that elastically-tethered elements could be more effective than comparable wire-tethered elements even though the former required deeper submergence to avoid broaching the surface. Although dissipation in the horizontal direction was actually less, this reduction was more than compensated for by an increased contribution in the vertical dimension. To simulate the response of the tethered element in irregular waves, we used the sum of thirteen randomly phased Fourier components as measured in a lake for the excitation. At a selected time interval, data was written to disk file for subsequent spectral analysis.

The previously discussed one and two-dimensional drag-force formulations were compared through simulation. C_D and C_M were assumed constant for each direction. Linear elongation of the elastic tether was varied over a range of values from 4% to 200%. Regardless of the elastic constant selected, response and dissipation varied no more than 10% in all cases tested; therefore, using the simpler, one-dimensional drag force formulation is an acceptable approximation for a linear model.

To discuss the relationship in irregular waves between relative velocity and energy dissipation requires a linearized model of dissipation so the phenomenon can be treated as a sum of Fourier components (6). Furthermore, complete linear analysis permits more design insight than the trial and error approach of simulation.

Linear analysis: The restoring forces in the equations of motion can be decoupled and linearized. Expressions for the water particle kinematics in a deep-water Airy wave can be simplified by assuming the spatial movement of the buoy will not substantially affect the water velocities and accelerations adjacent to the buoy.

Seymour (5) extended Jacobsen's (12) damping linearization to broadband irregular flows using a statistical approach and minimizing the difference in dissipation calculated by linear and non-linear models. The linearized drag term for the buoy drag is of the form DU_0u_r . U_0 is the "characteristic" relative velocity:

$$U_0 = 16\sigma_{u_r}/3\sqrt{2\pi} \quad (17)$$

where σ_{u_r} is the square root of the variance of relative velocity in one dimension. Seymour's approach was applied to linearizing the drag

of the tether. The linearized tether drag is of the form $D_t U_t \dot{x}$ where:

$$U_t = 16\sigma_x / 3\sqrt{2\pi} \quad (18)$$

Equations 9 and 10 in linearized form are written:

$$M\ddot{x} + [D'_x + D'_t]\dot{x} + K_x x = D'_x u + N\dot{u} \quad (19)$$

$$M\ddot{y} + [D'_y]\dot{y} + K_y y = D'_y v + N\dot{v} \quad (20)$$

where $D'_x = D_x U_0$ and $D'_t = D_t U_t$ (21)

$$K_x = (\rho V_0 - M_s)g/l_0 \quad K_y = k_t \quad (22)$$

Equations 19 and 20 are analogous; only operations on the first will be discussed. Lumping linearized drag terms ($D'' = D'_x + D'_t$) and taking the Laplace transform of each side of the Eq. 19, yields the transfer function of the buoy in the horizontal dimension:

$$H_x(s) = \frac{X(s)}{P(s)} = \frac{D's + Ns^2}{Ms^2 + D's + K_x} \quad (23)$$

The transfer function of relative velocity is:

$$H_{u_r}(s) = \frac{(N-M)s^2 - D_t's - K_x}{Ms^2 + D''s + K_x} \quad (24)$$

Changing from the Laplace transform to a Fourier transform, the predicted spectrum of horizontal relative velocity is:

$$S_{u_r}(\omega) = S_u(\omega) |H_{u_r}(\omega)| \quad (25)$$

where $S_u(\omega)$ is the spectrum of horizontal water particle velocity. The variance of relative velocity is calculated as:

$$\sigma_{u_r}^2 = \int_{-\infty}^{\infty} S_{u_r}(\omega) d\omega \quad (26)$$

The three previous equations are solved iteratively using estimates of the variances of buoy velocity \dot{x} and buoy relative velocity u_r to initiate the double transcendental solution.

Average drag power of a buoy over a frequency band is:

$$\bar{P}_{D_x}(\omega) = \frac{1}{2} D'_x U_r^2(\omega) \quad (27)$$

Therefore, $\bar{P}_{D_x}(\omega) = \frac{1}{2} D'_x S_{u_r}(\omega)$ (28)

Drag dissipation due to the tether is relatively small and therefore, neglected. Energy dissipation by a row of buoys is modeled over each averaged frequency band as the sum of the dissipation by Fourier components in each dimension.

$$\bar{x}(\omega) = \frac{1}{2} \beta \frac{[D'_x S_x u_r(\omega) + D'_y S_y v_r(\omega)]}{P_w(\omega)} \quad (29)$$

Knowing the transcendental solution to each equation, one can calculate the resonant frequencies of the system. Natural frequencies for a tethered buoy whose mass is small and respect to the displaced water and whose tether is a linear spring are written:

$$\omega_{nx} = \sqrt{g/(C_m l_o)} \quad \text{and} \quad \omega_{ny} = \omega_{nx} \sqrt{l_o/(l_o - r_o)} \quad (30)$$

where r_o is the unstretched tether length and l_o is its stretched length. Damping ξ is calculated as $D/2M\omega_n$. Resonant frequency is calculated according to the equation:

$$\omega_r = \omega_n \sqrt{1 - \xi^2} \quad (31)$$

The linearized model provides the analytical tool for matching the system response to predicted wave frequency by indicating the proper tether length and spring constant. The analysis indicates that vertical resonance will always be at a higher frequency than horizontal resonance. One possibility for altering this relationship may lie in using an ellipsoidal buoy so that the area exposed to the flow and the flow co-efficients are different in the horizontal and vertical dimensions.

FIELD TEST

The field test model was designed for installation about 100 yards off the northwest shore of Diamond Island in Lake Winnepesaukee, the largest lake in New Hampshire (See Fig. 6). The storm winds from the northwest had a six to nine mile fetch over which to build wave energy to test the system. We anticipated a maximum of three to four-foot significant waves with a three second peak period based upon the historical observation of long-time residents in the area.

The dynamic breakwater array: The breakwater float array was moored by a level steel frame anchoring grid designed by Vidal (13) with adjustable legs to level it on the bottom like a multilegged table. Buoys were then tethered to their anchoring frame so each tether was the same length. Such an anchoring system would not be practical for a working prototype system, but was used here because it provided an immobile base and simplified the subsequent analysis. It also focused the project on the effects of the elastic tethers and the floats. Such an anchoring frame was also consistent with the installation equipment, funds and talents available to us. The anchoring surface of the frame was 21 feet below the mean

free water surface after installation. The bottom sloped from approximately 27 feet to 35 feet from the shore side to the weather side of the frame.

The 90 floats in the array were 22 inch diameter plastic, inflatable, near-spherical floats. They were tethered with two parallel, one inch diameter solid rubber filaments as shown in Fig. 7. From previous work done by Savage (2,3) and our own tests of the spring constant for available solid rubber filaments, we had specified a filament with a linear spring constant of 15 lbs/foot elongation after initial loading to 120 pounds. However, the material we finally received did not meet specification by a wide margin. Its spring constant was about 35 lbs/foot elongation; so we were unable to obtain the desired magnitude of vertical response of the buoys in even the highest sea states. After discussions with several large manufacturers of rubber we have concluded that knowledge of rubber creep and elastic properties is not sufficiently complete to provide consistent and predictable material properties of the kind we have been seeking.

The array and instrumentation: Fig. 8 shows the plan and side views of the breakwater array that was installed at Lake Winnepesaukee and the location of wave staffs to measure the incident and attenuated waves. Details of the design of these transmission line wave staffs will be available in a publication by Winn, Stotz and Delano (14). As indicated in Fig. 8, one tether was instrumented to permit measurement of buoy motion response. Data from this buoy provided a check on our analytical models of dynamic response.

The effects of diffraction were not directly addressed in this experiment, but we believe such effects were not significant because our breakwater was not a thin, impervious wall. Also, the wave staff measuring the attenuated waves behind the breakwater was located in the middle and close to the breakwater as shown in Fig. 8. It would therefore have received the minimum possible energy transmitted by diffraction if there was any at all.

The greatest difficulty in the field experiment arose from the excessive creep of the rubber tethers that caused some of the floats to come to the surface, and these had to be pulled back down with shortened tethers to maintain design depth. It was here that the lack of quality control on the delivered rubber filaments showed up to seriously hinder the project, but the problem was overcome at the expense of greatly increasing the spring constant of the tethers which altered the breakwater vertical response from the original design.

RESULTS AND DISCUSSION OF THE FIELD EXPERIMENT

The least controllable aspect of the field experiment was the weather. Moderate cold fronts during the fall brought waves only as high as 2.0 feet significant height. A week before winter ice set in, waves 2.5 feet in significant height were recorded. The energy dissipation by the breakwater averaged over nine five-minute records from December 18, 1975 was 51%. Averaged over five records from November 5, it was 53%.

Several adjacent records from each day were selected for detailed analysis and modeling. Averaged incident and attenuated wave spectra measured over a ten-minute interval are shown in Fig. 9. Assuming rows were equally efficient, then each row dissipated about 8% of its incident wave energy.

Modeling buoy response and dissipation: In general, the measured horizontal buoy response was about five times greater than the vertical -- less than we had sought due to the undesirably high tether modulus.

C_D and C_M were estimated by matching the model results to the measured response of a wire-tethered buoy which was switched temporarily into the array so buoy response data with minimum cable drag could be acquired. The best correspondence between measured and modeled buoy motions was for a $C_D = 0.42$ and $C_M = 0.50$. These high values, coupled with the estimated rms a_T/d ratio of 0.65, indicated that the buoy wake was not fully developed as we had expected.

C_D and C_M of 0.42 and 0.50 respectively also yielded the closest fit between measured and modeled response for the elastically-tethered buoy. Fig. 10 compares the measured and modeled frequency response for several averaged records from December 18, and Fig. 11 makes the same comparison for the spectrum of horizontal relative velocities.

From horizontal and vertical spectra of relative velocity, the linearized drag power was computed over each frequency band in each spectrum. Results are compared with those measured in the field in Fig. 12. The lines of least-squares fit correspond in the region of highest energy density. Discrepancies at high frequencies may be due to breakdown of the model in that region. The results of the linear model correspond reasonably well with those of the coupled non-linear model.

CONCLUSIONS

From further investigation of the linear and non-linear models, it appears that their results are within 10% of one another for tether elongations from 0% to 30%, the measure of tether compliance used in our work. At 100% elongation, it appears most elastically-tethered systems can be more effective than their wire-tethered counterparts. However, their performance advantage is marginal because the buoys with more compliant tethers must be submerged deeper to avoid breaching the surface. Also the elastic tether is many times thicker than its wire counterpart and adds damping to the horizontal response; thereby reducing the energy dissipation by the buoy. Finally, it appears that a fully-developed wake (analogous to supercritical, steady flow) is not a necessary condition for maximum energy dissipation. Assuming that $C_D = 0.25$ and $C_M = 0.35$ characterize fully turbulent flow and that $C_D = 0.42$ and $C_M = 0.50$ characterize sub-critical turbulent flow, the models indicate that maximum dissipation by a tethered sphere system could be the same for each flow regime. However, the optimum tether length would be different for a given buoy operating in one flow regime or the other.

In summary, we found it was possible to remove 50% of the wave energy using a nine-row array of tethered buoys, and that we could model the

energy dissipation fairly accurately. Our test of the performance advantage of elastic tethers was not conclusive because of manufacturing problems and present state-of-the-art limitations. Our understanding of relationships between wake development and buoy size relative to wave parameters over a range of scales in two-dimensional oscillatory flow is incomplete.

ACKNOWLEDGMENTS

The principal support for this project from the National Sea Grant Program (Grant No. 04-5-158-50) is gratefully acknowledged. Valuable information and contributions were also received from previous related research, notably the Office of Naval Research Contract No. N00014-67-A-0158-0004 and the United States Coast Guard Research and Development Contract No. 4-20050-000.

REFERENCES

1. Seymour, R. J., and J. O. Isaacs, Tethered float breakwaters, Proceedings of First Int'l. Conf. on Floating Breakwaters, Univ. of Rhode Island, Newport, R.I., April, 1974.
2. Savage, G. H., and J. B. Hersey, Project Seaspider, Reference No. 6842, Woods Hole Oceanographic Institution, Woods Hole, Mass., June, 1968.
3. Savage, G. H., Testing rubber band filaments as buoy moorings for some test navigation buoys, Engineering Design and Analysis Laboratory Report, Univ. of New Hampshire, Ourham. Letter Report to United States Coast Guard Research and Development Center, Contract No. 4-20050-000, November 9, 1973.
4. Demos, S. E., G. A. Stewart, and R. W. Corell, A computer study of the hydrodynamic loading of a compliant taut-wire mooring, EOAL Tech. Rpt. #109, University of New Hampshire, July, 1970.
5. Seymour, R. J., Resistance of spheres in oscillatory flows, Ph.D. Dissertation, Univ. California, San Diego, 1974.
6. Agerton, O. J., The design, analysis and field test of a dynamic floating breakwater. Ph.D. Dissertation, Univ. of New Hampshire, Ourham, Dec. 1976.
7. Morison, J. R., J. W. Johnson, M. P. O'Brien, and S. A. Schaaf, The forces exerted by surface waves on piles, Petroleum Trans., Vol. 189, TP2846, 1950.
8. Keulegan, G. H., and L. H. Carpenter, Forces on cylinders and plates in an oscillating fluid, J. Res. National Bur. Standards, 60, 5, May, 1958.

9. Sarpkaya, T., Forces on cylinders and spheres in a sinusoidally oscillating fluid, J. Applied Mechanics, ASME, March, 1975.
10. Laird, A. D. K., Water forces on flexible oscillating cylinders, J. Waterways Harbors Div., Proc. ASCE, Vol. 88, WW3, August, 1962.
11. Stotz, K. C., D. O. Libby, and G. H. Savage, Computer model and data interpretation for a rubber cable tethered wave amplitude measuring buoy, Proc. Ocean 75 Conf., IEEE and MTS, San Diego, 1975.
12. Jacobsen, L. S., Steady forced vibration as influenced by damping, Trans. ASME, Vol. 52, no. APM 52-15, 1930.
13. Vidal, D. A., Design, analysis, construction, and installation of a floating breakwater anchoring system and related structures. Master of Science Project Report, Univ. of New Hampshire, 1975.
14. Winn, A. L., Stotz, K. C., Delano, J. R., The design and field operation of a transmission-line wave staff. (In preparation), University of New Hampshire.
15. Winn, A. L., G. H. Savage, and R. R. Hickman, Design and instrumentation of a shore-recording wave amplitude measuring buoy, Proc. Ocean 75 Conf., IEEE and MTS, San Diego, 1975.

NOMENCLATURE

a	amplitude	r_0	unstretched tether length
A	area	$S_z(\omega)$	spectrum of z
a_r	amplitude of buoy displacement relative to water particle displacement	s	Laplace operator
B	constant	T	tension in tether
D	Lumped drag constant of form $\frac{1}{2} \rho A C_D$	t	time
D'	Lumped drag constants of form $\frac{1}{2} \rho A C_D U_0$	U_r, V_r	horizontal and vertical relative velocity respectively
D''	Lumped linearized drag constant including buoy and tether drag	U_0, V_0	"characteristic" relative velocity - linearization constants
d	diameter	u, v	water particle velocity
F_B	force of buoyancy	\dot{u}, \dot{v}	water particle acceleration
g	acceleration of gravity	U_m	maximum relative velocity
H	wave height	V_0	displaced volume
$H_x(\omega), H_y(\omega)$	linearized transfer functions	x, y	horizontal and vertical displacements respectively
k_x, k_y, k_z	lumped restoring force constant	z	depth of submergence
k	wave number	z (subscript)	refers to horizontal water particle position
k_t	spring constant for tether	β	buoy packing density (#/ft.)
l_0	tether length for buoy at rest	λ	energy dissipation per row
M	lumped mass constant: $M_b + M_s$	ρ	density of water
M_s	mass of sphere	ξ	damping coefficient
M_w	mass of displaced water	ω	frequency (radians/sec)
N	lumped mass constant: $M_w(1+\mu)$	ω_n, ω_r	natural and resonant frequency
n	number of rows	θ	angle of tether from vertical
P_D	drag power	σ^2	variance
P_W	wave power	$\langle \cdot \rangle$	average value
R	stretched tether length	$\{ \cdot \}$	absolute value
\vec{r}	vector relative velocity		

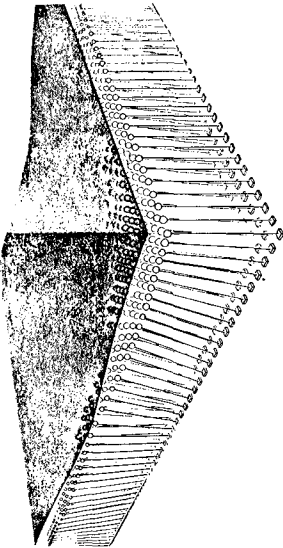


Fig. 1 Seymour and Isaacs tethered float breakwater (1).

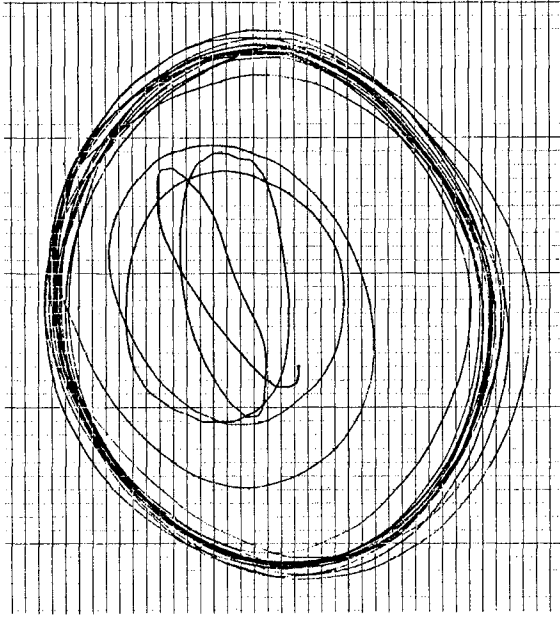


Fig. 2 Orbit of elastically-tethered buoy as tracked by optical instrumentation in wave tank tests.

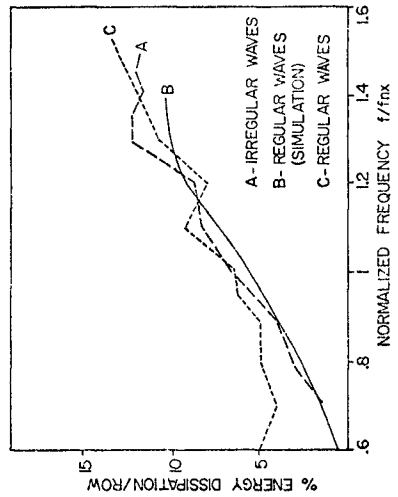


Fig. 4 Measured and modeled performance of scale model elastically-tethered array.

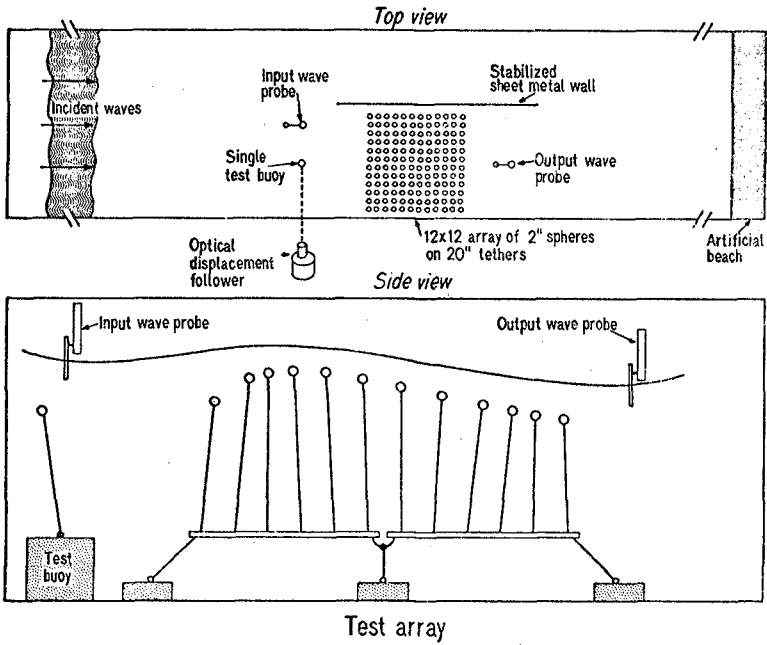


Fig. 3 Top and side views of wave tank tests.

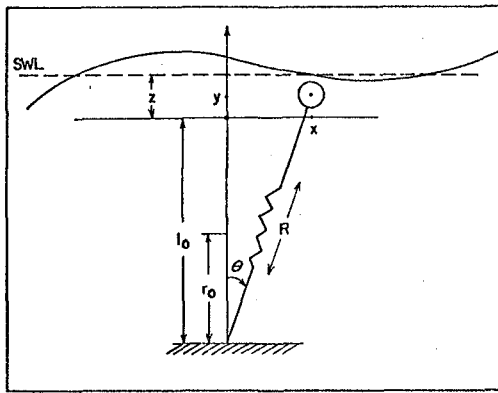


Fig. 5 Geometry of elastically-tethered buoy.

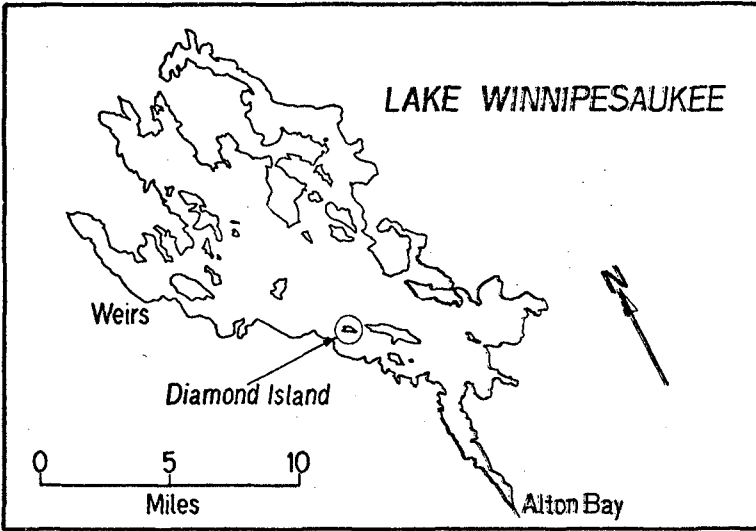


Fig. 6 Diamond Island, site of the field experiment.

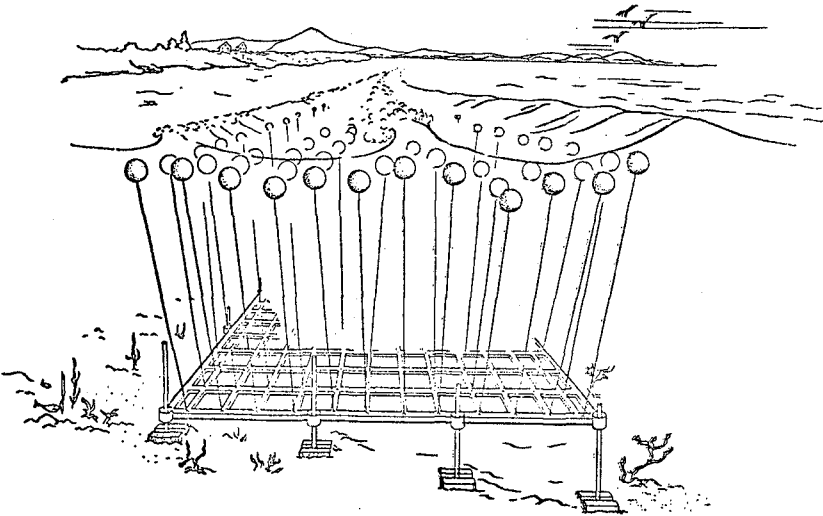
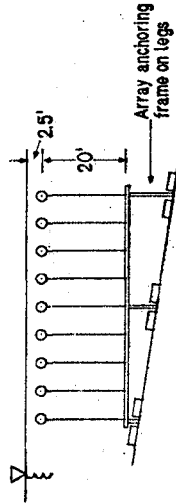
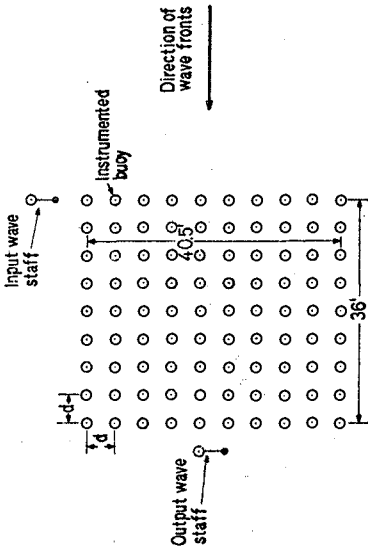


Fig. 7 Elastically-tethered test array for lake field test.



Breakwater array:
 Number of rows: 9
 Number of columns: 10
 Buoy diameter: 2'
 Spacing (d): 4.5'

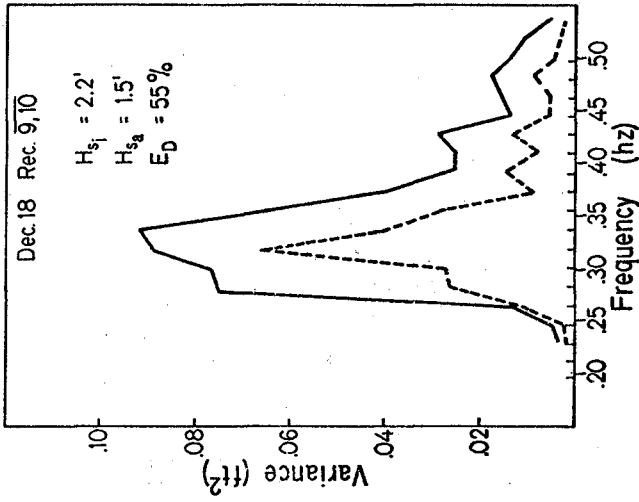


Fig. 9 Measured incident and attenuated wave spectra.

Fig. 8 Layout of field-test array and instrumentation.

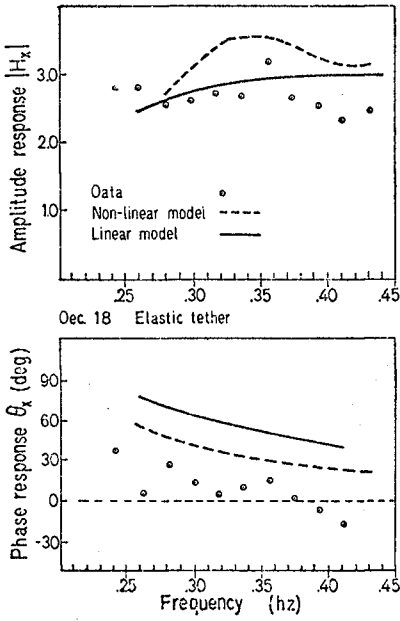


Fig. 10 Horizontal frequency response.

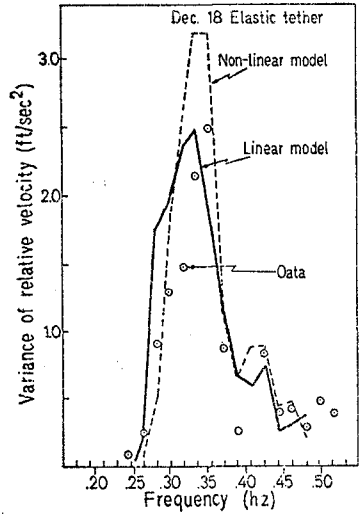


Fig. 11 Spectra of horizontal relative velocity.

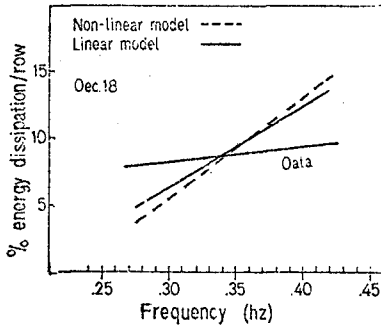


Fig. 12 Breakwater performance.